CHEMISTRY OF MATERIALS

ARTICLE

pubs.acs.org/cm

Structure versus Thermal Stability: The Periodic Structure of Atomic Layer Deposition-Grown Al-Incorporated HfO_2 Films and Its Effects on Amorphous Stabilization

Tuo Wang and John G. Ekerdt*

Department of Chemical Engineering, The University of Texas at Austin, Austin, Texas 78712, United States

ABSTRACT: Atomic layer deposition (ALD) is used to grow Al-incorporated HfO_2 to study the relationship between the film composition variations in the growth direction and thermal stability of the amorphous phase. Ten nm films with Hf:Al ALD cycle ratios equal to 3:1 and 8:1 remain amorphous up to 900 and 800 °C, respectively, and crystallize after a 30 s annealing at 950 and 850 °C, respectively. Angle-resolved X-ray photoelectron spectroscopy is used to reveal the periodicity of ALD-grown Al-incorporated HfO_2. Generally, multiple cycles are required to realize a complete layer in ALD. Films with a Hf:Al ALD cycle ratio of ≥5 have a periodic $HfO_2-HfAl_xO_y$ structure, while films with a Hf:Al ALD cycle ratio of <4 appear more like homogeneous films. Increasing the thickness of a homogeneous-like film (Hf:Al = 3:1 ALD cycle ratio) from 10 to 40 nm leads to crystallization when annealed at 900 °C. Amorphous films with a periodic structure (Hf:Al = 8:1, ALD cycle ratio) do not display a dependence of crystallization on film thickness at the same 800 °C annealing condition. The factors controlling the film thermal stability are not only the overall amorphzier incorporation concentration but also how the amorphizer is distributed in the film. Changing the periodic structure of an ALD-grown Al-incorporated HfO_2 film is a potential method to tune the film thermal stability.

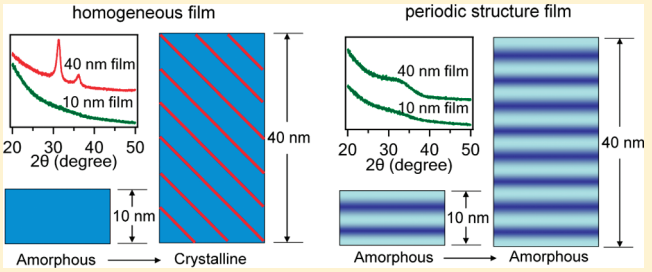

KEYWORDS: coatings, thin films, monolayers, electronic materials, microstructure

1. INTRODUCTION

In recent years, HfO_2 has attracted considerable attention as a dielectric material to replace conventional SiO_2 because of its high dielectric constant ($k \sim 20$), high bandgap of ~5.5 eV and relatively good stability on silicon.[1−5] Unfortunately, amorphous HfO_2 crystallizes after annealing at a relatively low temperature (~500 °C).[2] Although crystalline HfO_2 has a higher dielectric constant, stabilizing HfO_2 in its amorphous phase is more desirable because the polycrystalline film grain boundaries serve as a charge leakage pathway and the coexistence of cubic, tetragonal, and monoclinic phases results in different dielectric constants among different regions of the device.[1,6,7] Extensive effort has been made to stabilize the amorphous phase of HfO_2, including using new precursors to grow more robust amorphous HfO_2 and alloying HfO_2 with amorphizing elements, such as Si, Al, and La. Atomic layer deposition (ALD)-grown HfO_2 films using a heteroleptic precursor were found to have higher crystallization temperatures because of the increased Hf density.[8] Sputtering, chemical vapor deposition (CVD), and atomic layer deposition (ALD) have been used to incorporate Si,[9−13] Al,[14−19] and La,[20−22] respectively. Both film thickness and alloy composition need to be considered in evaluating the effectiveness of an alloying element in stabilizing the amorphous phase of HfO_2.

The amorphous nature of HfO_2 is different from SiO_2 in terms of the network structure. Thermally grown SiO_2 has a continuous random network (CRN), while HfO_2 has a random close packed (RCP) structure.[23] The differences between the two types of amorphous structure are related to the molar volume and the coordination number vs the metal−oxygen (M−O) distance,[24] as well as the electronegativity difference between M and O and average bond ionicity.[25] Generally speaking, a CRN material is a stronger amorphizer than a RCP material. While forming a CRN structure, each atom in SiO_2 is bonded according to its primary chemical valence and predominantly forms covalent bonds.[25] The Si−O covalent bonds in SiO_2 make SiO_2 a very stable amorphous material. The Hf−O bond in HfO_2 is predominantly ionic;[26] thus, O atoms can move around more easily in HfO_2 compared with O atoms in SiO_2. Therefore, HfO_2 has a much lower crystallization temperature than SiO_2.

La_2O_3 forms a RCP structure, and incorporating La into HfO_2 has been shown to be effective in stabilizing the amorphous phase.[20,21] Although La is a much weaker amorphizer compared with Si, La incorporation does not decrease the dielectric constant of the alloyed film as found with SiO_2.[20,21] While La_2O_3 and Y_2O_3 are both classified in the RCP group, La is an amorphizer but Y is a crystallizer. Y-incorporation stabilizes the higher dielectric constant cubic HfO_2 phase.[27−29]

According to Zallen's classification, there is a group of modified continuous random network (MCRN) materials between CRN and RCP, in which metal atom ionic bonds disrupt

Received: July 23, 2010
Revised: January 26, 2011
Published: March 01, 2011

and modify the covalently bonded CRN structure.[25] Al_2O_3 and Ta_2O_5 are examples of MCRNs. Elements forming CRN, MCRN, or RCP all show potential to stabilize the amorphous phase of high-*k* dielectric thin films; thus, the choice of incorporating elements involves an optimization/compromise between a stronger amorphizer and a higher dielectric constant. The film crystallization temperatures at a particular alloying element incorporation level are reported,[13,18,30,31] but it is sometimes difficult to compare these temperatures because different film thicknesses are employed.

Thermal stability is closely related to film thickness. Cho et al. reported that, while as-deposited 45 Å thick HfO_2 was amorphous, thicker films were grown as a polycrystalline structure of monoclinic or tetragonal phases.[32] Gusev et al. reported the dependence of film crystallization temperature on the thickness of HfO_2 films. The crystallization temperature decreased from 600 to 430 °C with thickness increases from 5 to 40 nm.[2] HfO_2 grown from a $HfCl_4$ precursor showed similar behavior; the 300 °C grown as-deposited thinner (50 ALD cycles) film was amorphous whereas thicker (100, 150, and 200 ALD cycles) films were more crystalline.[33] For HfO_2 films alloyed with another element, 12 nm thick Al-incorporated HfO_2 contained both tetragonal and monoclinic phases after high temperature annealing, whereas 3 nm thick Al-incorporated HfO_2 crystallized into the monoclinic phase.[34]

The overall energy of a film is determined by the contributions from both the bulk and the surface. Crystalline films have a lower energy than amorphous films, but Navrotsky revealed that monoclinic HfO_2 and ZrO_2 were found to have the largest surface enthalpy and amorphous HfO_2 and ZrO_2 have the smallest.[35] As film thickness decreases, the surface energy of the amorphous phase makes a greater contribution to the total energy, which enables the film to remain amorphous. This is the reason why thinner, as-deposited HfO_2 is generally amorphous while thicker films are generally crystalline.

Physical sputtering, CVD, ALD, and molecular beam epitaxy (MBE) growth are the most commonly used methods to incorporate alloying elements into HfO_2. Our previous work showed the existence of a periodic structure resulted from inserting one ALD layer of La_2O_3 between several ALD layers of HfO_2.[36] Less La was required to stabilize an amorphous phase for the $HfLa_xO_y$ system when present in a periodic structure as compared to homogeneous films grown by physical sputtering.[21] Katamreddy et al. report $HfAlO_x$ films grown with 4:2 and 2:1 Hf:Al ALD cycle ratios have different degrees of crystallization after annealing under the same condition, implying the thermal stability is determined by film structure rather than overall Al content.[37] $HfO_2-Al_2O_3$ nanolaminate films with clear interfaces also demonstrate a structure dependent thermal stability. 100 nm thick $HfO_2-Al_2O_3$ nanolaminate films composed of a repeated [3 nm HfO_2 + 3 nm Al_2O_3] structure remain amorphous after 700 °C annealing, whereas samples composed of repeated [4 nm HfO_2 + 4 nm Al_2O_3] and [10 nm HfO_2 + 10 nm Al_2O_3] structures crystallize into tetragonal and a mixture of monoclinic/tetragonal phases under the same annealing condition.[38] Therefore, the film structure in the growth direction, defined by ALD, shows the potential to be another factor affecting the crystallization temperature of thin films.

In this paper, Al-incorporated HfO_2 (denoted as Al-HfO_2) films are synthesized using ALD to study the relationship between the periodic structure and the film crystallization behavior. Using ALD to incorporate Al into HfO_2 for amorphous stabilization has been widely reported and is not our major concern. The periodic structures are characterized using angle-resolved X-ray photoelectron spectroscopy (AR-XPS). Films are annealed using a rapid thermal annealing (RTA) process. The crystallization of films with comparable compositions and different thicknesses are studied using grazing incidence X-ray diffraction (GIXRD).

2. EXPERIMENTAL SECTION

2.1. Film Deposition. Samples are deposited on n-Si(100) substrates at 250 °C using tetrakis (ethylmethylamino) hafnium Hf[N-$(CH_3)(C_2H_5)]_4$ (TEMAH), trimethyl aluminum (TMA), and H_2O; the TEMAH is held at 85 °C. TMA and H_2O are at room temperature. A detailed ALD reactor description is reported elsewhere.[21] One cycle consists of metal precursor dosing for 1.5 s (Hf) or 0.75 s (Al), a 25 s purge with Ar, water dosing for 0.05 s, and a 25 s purge with Ar. The growth rate of HfO_2 and Al_2O_3 in our ALD system is 0.78 and 0.90 Å/cycle, respectively. The Si substrates are etched in a 2% HF solution for 30 s, rinsed in deionized water for 20 s, which reoxidizes the Si(100) surface, and dried with flowing He. The resultant oxide is 10 Å according to ellipsometry. The Al incorporation is achieved by growing HfO_2 and Al_2O_3 alternately; one ALD layer of Al_2O_3 is added after *x* ALD layers of HfO_2, and then, this sequence is repeated *n* times to achieve the desired thickness. Films are referenced using [*x*Hf + 1Al] × *n*. Film growth always ends with an *x*Hf cycle. One "ALD layer" does not imply a complete monolayer of a particular material, and we refer to an ALD layer as the amount deposited in a single cycle. Samples of two target thickness are deposited, 10 and 40 nm. The as-deposited samples are confirmed to be 11 or 41 nm (10 or 40 nm high-*k* film + 1 nm interfacial SiO_2) by ellipsometry.

2.2. X-ray Photoelectron Spectroscopy (XPS). After cooling down in the ALD chamber, the as-deposited samples are transferred to a Physical Electronics 5500 XPS system through a load lock with a base pressure of 2×10^{-7} Torr. In situ XPS and AR-XPS are performed using a Mg Kα source at 1253.6 eV to investigate the overall film composition and depth composition variation. The angle between the X-ray source and the photoelectron analyzer is 54.7°. The normal take off angle (between the analyzer and the sample surface) is 45°, at which XPS is normally performed. AR-XPS is achieved by tilting the sample in a set of planes perpendicular to the plane defined by the X-ray source and the analyzer. The sample position has been calibrated so that the tilt axis crosses the intersection point of the X-ray and the analyzer.

The XPS raw data are smoothed using PeakFit (Version 4) to find the starting and ending points for integration; the peak area of the raw data is calculated using the Igor Pro software package. The XPS data are presented as ratios of the (Al 2p)/(O 1s) peak areas. Al 2p XPS raw data smoothing is most difficult at very small take off angles where the signal-to-noise ratios are low, because the choice of the starting and ending points for the integration lead to variations large enough to affect the calculated (Al 2p)/(O 1s) area ratios. To check the reproducibility of the analysis method, five measurements at five different take off angles (7, 12, 18, 22, and 26°) were performed for the [4Hf + 1Al] sample. The error bars are presented (in Figure 3c), and after 12°, the signal-to-noise ratios for Al 2p and O 1s are big enough such that the error bars are smaller than the vertical segment of the data point symbols.

2.3. Annealing and X-ray Diffraction (XRD). To find the film crystallization temperature, samples are annealed by rapid thermal annealing (RTA) at different temperatures for 30 s under a N_2 environment. Grazing incidence X-ray diffraction (GIXRD) is performed using a Bruker-AXS D8 Advance Powder Diffractometer with sealed tube Cu Kα radiation, at a fixed 0.5° incident angle and 2θ scan rate of 6°/min.

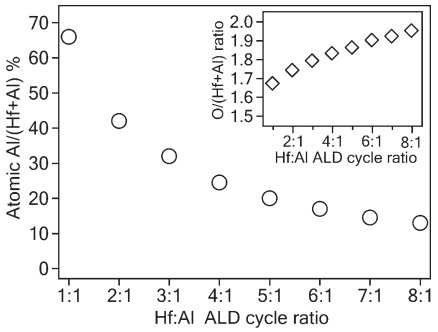

Figure 1. Al-incorporation level of as-deposited Al-HfO_2 films versus Hf:Al ALD cycle ratio. Inset: atomic O/metal ratio is calculated from the O/(Hf + Al) XPS peak areas.

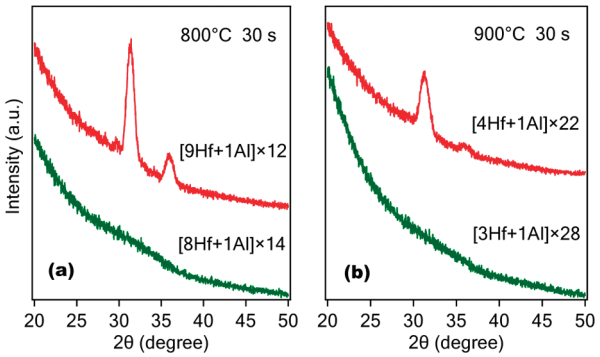

Figure 2. XRD spectra showing the minimum Al-incorporation levels for 10 nm Al-HfO_2 films to remain amorphous after 800 and 900 °C annealing for 30 s in a N_2 environment.

3. RESULTS AND DISCUSSION

3.1. Amorphous Stabilization of 10 nm ALD-Grown Al-HfO_2 Films. Only Hf, Al, O, and C peaks are observed in the X-ray photoelectron spectra of Al-HfO_2 samples. Carbon contamination is introduced to the samples within the load lock during in situ sample transfer. No C signal is detected after Ar^+ sputtering at 3 kV over a 3 × 3 mm^2 area for 40 s, which removes ~2 nm of the sample surface, indicating the C impurities in the bulk film are below the XPS detection limits (<1%). The as-deposited film composition is calculated from the integrated Hf 4f, Al 2p, and O 1s peaks corrected by their atomic sensitivity factors.[39] Figure 1 shows the Al-incorporation level of a series of 10 nm, as-deposited films at different Hf:Al ALD cycles ratios. The atomic O/metal ratio of the eight samples is calculated from the O/(Hf + Al) XPS peak areas and is shown in the inset.

Consistent with previous studies,[18,19] Al is successfully incorporated into HfO_2 using ALD, and the Al concentration can be easily controlled by changing the Hf:Al ALD cycle ratios. When the Hf:Al ALD cycle ratio is 1:1, the Al incorporation concentration is 66% on a metal basis, indicating more Al precursors than Hf precursor adsorbed onto the sample surface during the metal precursor dosing step as expected because the TMA molecule is about three times smaller than TEMAH. When the Hf:Al ALD cycle ratio is 8:1, the Al incorporation level is about 13%. The atomic O/metal ratio gradually approaches 2.0 as the sample becomes an HfO_2 dominant film as the Hf:Al ALD cycle ratio changes from 1:1 to 8:1.

To investigate the stabilization effects of Al-incorporation, another set of 10 nm Al-HfO_2 films with various Al-incorporation levels were deposited and then annealed. XRD measurements illustrate the minimum Al-incorporation levels that are needed to stabilize the amorphous phase after 800 and 900 °C annealing, respectively. When one ALD Al_2O_3 layer is inserted after every eight ALD HfO_2 layers (Al/(Hf + Al) = 13%), the 10 nm [8Hf + 1Al] × 14 film remains amorphous after 800 °C annealing. Adding one more ALD layer of HfO_2 in every [xHf + 1Al] sequence while keeping the same 10 nm film thickness, the [9Hf + 1Al] × 12 film crystallizes at 800 °C as indicated by the two peaks at 2θ = 31 and 36° in the XRD spectrum (Figure 2a). These two peaks are close to tetragonal (111) and tetragonal (002) for HfO_2. Similarly, a 10 nm [3Hf + 1Al] × 28 (Al/(Hf + Al) = 32%) remains amorphous as high as 900 °C, but a 10 nm [4Hf + 1Al] × 22 film crystallizes after annealing at the same temperature (Figure 2b).

Generally, a higher Al-incorporation level increases the thermal stability of Al-HfO_2 films,[18,40] which is related to the changes in the Al−O and Hf−O bonding characteristics during the incorporation of Al_2O_3 into HfO_2.[19] In our case, 13% ([8Hf + 1Al]) and 32% ([3Hf + 1Al]) Al-incorporation stabilizes the amorphous phase up to 800 and 900 °C, respectively, using a RTA process for 30 s under a N_2 environment. It is widely reported that Al-HfO_2 can remain amorphous at an annealing temperature higher than 900 °C,[18,31,40] which is close to the rapid thermal processing range in the device manufacturing processes.[41]

3.2. Periodicity of ALD-Grown Al-HfO_2 Films. Unlike ALD-grown HfO_2−Al_2O_3 nanolaminates, which are composed of thicker HfO_2 and Al_2O_3 stacks in the thickness of several angstroms,[42,43] it is more difficult to characterize the periodicity of the films used herein since only one ALD layer of Al_2O_3 is inserted and this will not form a complete monolayer of Al_2O_3. Direct methods are less likely to work in characterizing the periodicity of Al-HfO_2 films grown in [xHf + 1Al] sequences. We performed TEM and XPS depth profiling (Ar^+ sputtering) for our [xHf + 1La] system.[36] No repeated periodic features were observed in TEM even for samples with large x values (e.g., [9Hf + 1La]), and no compositional variation was observed in XPS depth profiling analysis because the repeated structures are extremely thin (<8 Å). AR-XPS has been shown to be a powerful nondestructive tool to determine the thickness, fractional coverage, and concentration depth profile for ultrathin films.[44−46] The detected XPS signal is given by $I = I_0\exp(-d/\lambda\sin\theta)$. Lambda, λ, is the effective attenuation length (EAL),[47] and θ is the take off angle between the analyzer and the sample surface. At small take off angles, only photoelectrons from the near surface region are detectable.[46] Although the periodicity of ALD-grown Al-HfO_2 films is smaller than the EAL, at glancing take off angles, the abrupt presence of the first few $HfAl_xO_y$ layers is expected to be detectable using the AR-XPS technique. Here, $HfAl_xO_y$ in the context of $HfAl_xO_y$−HfO_2 refers a certain thickness composed of a HfO_2 and Al_2O_3 mixture and HfO_2 refers to certain thickness composed only of HfO_2.

For each sample, AR-XPS is conducted from near grazing to 45° take off angles. Figure 3a shows the result of a 10 nm pure Al_2O_3 film. The (Al 2p)/(O 1s) value is high initially because of the scattering effects of the photoelectrons. At near grazing take off angles, photoelectrons may escape from the surface by a shortcut, enabling signals from deeper depths to be detected.[48] This effect is more significant for Al 2p as the EAL(Al 2p) > EAL(O 1s). After 12°, the take off angle is large enough and the scattering effects no longer play an important role, so the (Al 2p)/(O 1s) ratio remains reasonably constant as the film is wholly composed of Al_2O_3.

dx.doi.org/10.1021/cm102057d |Chem. Mater. 2011, 23, 1679–1685

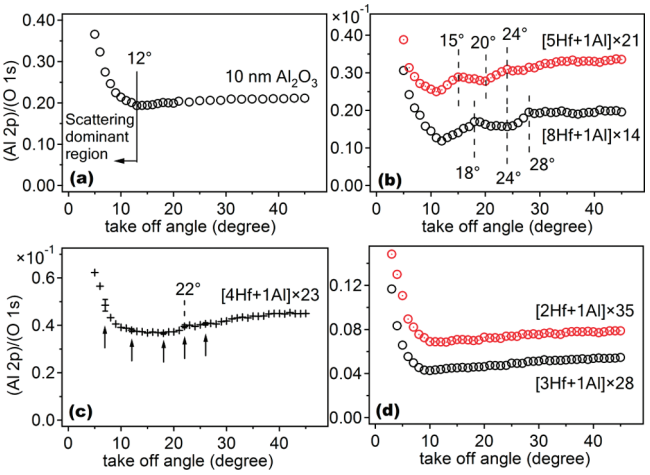

Figure 3. (Al 2p)/(O 1s) photoelectron intensity ratios of (a)10 nm Al_2O_3; (b) [8Hf + 1Al] × 14 and [5Hf + 1Al] × 21; (c) [4Hf + 1Al] × 23; (d) [3Hf + 1Al] × 28 and [2Hf + 1Al] × 35 films; error bars at 7, 12, 18, 22, and 26° for the [4Hf + 1La] × 23 sample are shown at the corresponding data points, respectively.

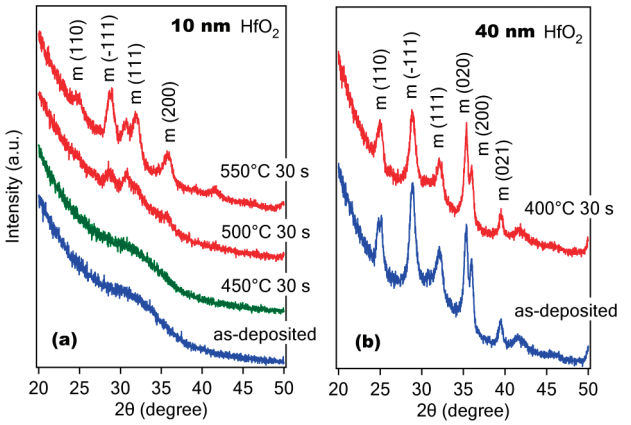

Figure 4. XRD spectra of (a) 10 nm as-deposited HfO_2 and HfO_2 annealed at 450, 500, and 550 °C; (b) 40 nm as-deposited HfO_2 and HfO_2 annealed at 400 °C.

Figure 3b shows AR-XPS results for samples with high Hf:Al ALD cycle ratios (8:1 and 5:1). For the [8Hf + 1Al] × 14 sample, the (Al 2p)/(O 1s) curve shows the same initial decrease as did pure Al_2O_3 (Figure 3a) below 12°, which is caused by the scattering effects at near grazing take off angles. After 12°, the (Al 2p)/(O 1s) curve does not remain constant as found for pure Al_2O_3. The curve increases at 12° < θ < 18° and then slowly decreases at 18° < θ < 24°, followed by another increase at 24° < θ < 28°. After 28°, the features become too small to identify. The increase at 12° < θ < 18° indicates that more and more Al is sampled in this depth region, illustrating the existence of an Al-rich $HfAl_xO_y$ layer different from the layer defined by the 18° < θ < 24° region. From 18° to 24°, the decrease of the (Al 2p)/(O 1s) ratio indicates that the corresponding depth region is either Al-free or at least has a very low Al concentration. Considering that ALD-grown HfO_2 using the same Hf precursor exhibited a Hf coverage of ~29% monolayer coverage/cycle,[49] we refer to this region as Al-free because 8 ALD cycles of HfO_2 are deposited between Al_2O_3 cycles in the [8Hf + 1Al] sample. The amount of Al atoms being detected stops increasing after the probing depth (EAL × sin θ) penetrates the above Al-rich $HfAl_xO_y$ layer that corresponds to 12° < θ < 18°, defining an Al-free HfO_2 layer that corresponds to 18° < θ < 24° where more O 1s signal is detected from HfO_2 in this depth region, decreasing the (Al 2p)/(O 1s) ratio. The increase at 24° < θ < 28° implies another Al-rich $HfAl_xO_y$ layer under the Al-free HfO_2 layer. After 28°, the trend of the curve becomes unresolvable because the probing depth (EAL × sin θ) is too deep that the periodicity is averaged. The (Al 2p)/(O 1s) curve for a 10 nm [5Hf + 1Al] × 21 shows the same trend as the 8:1 sample after 12°. The only difference is that the features appear over smaller angle ranges and move to the left because the repeated structure is thinner in this sample. The two increase segments at 11° < θ < 15° and 20° < θ < 24° represent two Al-rich $HfAl_xO_y$ layers. The decrease at 15° < θ < 20° can be attributed to an Al-free HfO_2 layer as the decrease in magnitude is similar to that of the [8Hf + 1Al] sample and 5 ALD cycles of HfO_2 are enough to form a HfO_2 monolayer. Inserting one ALD layer of Al_2O_3 after every five ALD layers of HfO_2 still ensures a periodic structure. Therefore, the features after 12° in Figure 3b reveal a nonuniform structure composed of an Al-free HfO_2 layer sandwiched between two $HfAl_xO_y$ layers. Although the features disappear when the take off angle is too large, it is reasonable to conclude these two films possess periodic structures considering the layer-by-layer nature of ALD growth.

For the 10 nm [4Hf + 1Al] × 23 sample in Figure 3c, no apparent features are developed similar to those in Figure 3b. The curve does show some inflections, such as the increase around 22°. The error bars are significant at 7° and are smaller than the vertical line segments of the data symbols for take off angles ≥12°. Thus, the feature at 22° represents an (Al 2p)/(O 1s) curve increase, which implies an Al concentration increase along the film growth direction. Compared with the two samples in Figure 3b, the [4Hf + 1Al] sample has thinner repeated layers; therefore, its features on the (Al 2p)/(O 1s) curve should be compressed over smaller angle ranges and move to the left even more than [5Hf + 1Al]. The increase around 22° for the [4Hf + 1Al] sample might be the same feature as the increase shown at 20° < θ < 24° and 24° < θ < 28° for the [5Hf + 1Al] and [8Hf + 1Al] sample, respectively. Other possible features, which are the counterpart to the 11° < θ < 15° feature for the [5Hf + 1Al] sample and the 12° < θ < 18° feature for the [8Hf + 1Al] sample, are shifted to the left and abut the scattering-effect-dominant region and become unresolved. The increase at 22° implies periodic structures start to develop in the [4Hf + 1Al] × 23 sample but have not completely formed.

Figure 3d shows the (Al 2p)/(O 1s) curves for the 10 nm [3Hf + 1Al] × 28 and [2Hf + 1Al] × 35 samples. No feature is observed except the initial decrease due to the scattering effects, implying these two samples are more like homogeneous films. On the basis of this AR-XPS analysis, we conclude that Al-free HfO_2 layers start to develop when the Hf:Al ALD cycle ratio is four and complete formation when the ratio equals five or larger, indicating the existence of periodic structures, while those smaller than four are more like homogeneous films.

3.3. Structure versus Thermal Stability. Knowing structural periodicity exists in films with high Hf:Al ALD cycles ratios (≥5:1), the relationship between film structure and thermal stability was studied. The crystallization behavior of thin (10 nm) and thick (40 nm) pure HfO_2 films is shown in Figure 4. Ten nm HfO_2 is amorphous as deposited at 250 °C, remains amorphous up to 450 °C, and crystallizes into the monoclinic phase between

dx.doi.org/10.1021/cm102057d |Chem. Mater. 2011, 23, 1679–1685

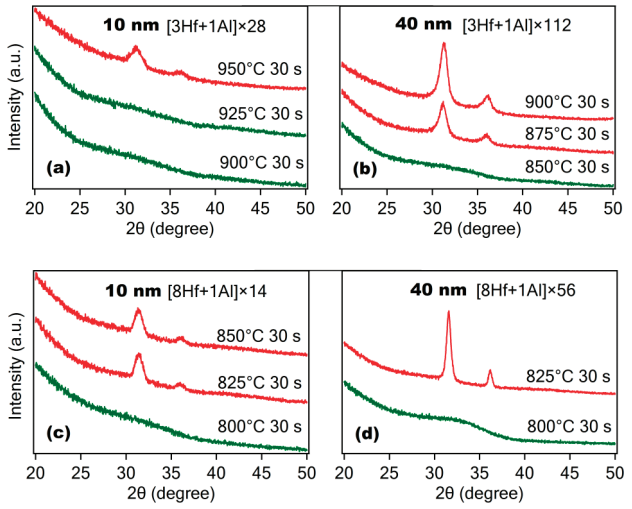

Figure 5. XRD spectra of (a) 10 nm and (b) 40 nm [3Hf + 1Al] films annealed at different temperatures and (c) 10 nm and (d) 40 nm [8Hf + 1Al] films at different temperatures.

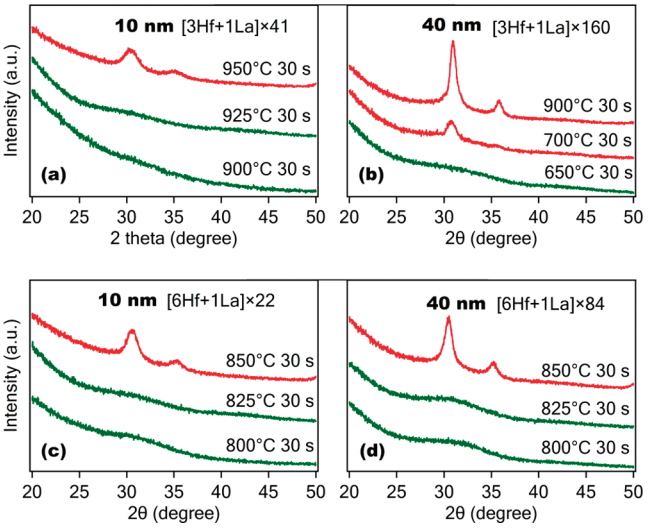

Figure 6. XRD spectra of (a) 10 nm and (b) 40 nm [3Hf + 1La] films annealed at different temperatures and (c) 10 nm and (d) 40 nm [6Hf + 1La] films annealed at different temperatures.

450 and 500 °C. The diffraction peaks at 2θ = 24.6, 28.5, 31.8, 35.6° can be assigned to the monoclinic phase, as marked in Figure 4a. With increasing thickness, HfO_2 is much easier to crystallize as the surface enthalpy contributes less to the total film energy. A 40 nm HfO_2 film crystallized into the monoclinic phase during growth at 250 °C. Annealing at 400 °C does not change the film phase, as shown in Figure 4b. The thickness dependent crystallization of HfO_2 is consistent with the results in refs 2, 33, and 34.

For ALD-grown Al-HfO_2 films with a structure more like homogeneous films, the film thermal stability is highly affected by alloy composition and film thickness. The 10 and 40 nm [3Hf + 1Al] films show thickness dependent crystallization characteristics. The 10 nm [3Hf + 1Al] remains amorphous after 900 and 925 °C, 30 s annealing and crystallizes at 950 °C, as shown in Figure 5a. A 40 nm thick film with the same [3Hf + 1Al] composition loses its thermal stability after 875 °C, 30 s annealing, as shown in Figure 5b. The crystallization onset temperature of the [3Hf + 1Al] films decreases from 925−950 to 850−875 °C as the film thickness increases from 10 to 40 nm. Similarly, a 10 nm [2Hf + 1Al] film is amorphous at 960 °C and crystallizes at 990 °C, whereas a 40 nm [2Hf + 1Al] film crystallizes at 960 °C (figure not shown).

However, for films with a periodic structure, the thermal stability becomes independent of thickness up to 40 nm. A 10 nm [8Hf + 1Al] × 14 film remains amorphous after 800 °C, 30 s annealing and crystallizes after 825 °C, 30 s annealing (Figure 5c). Unlike [3Hf + 1Al] films, a 40 nm [8Hf + 1Al] × 56 still remains amorphous after 800 °C, 30 s annealing, as shown in Figure 5d. The crystallization onset temperature of both the 10 and 40 nm [8Hf + 1Al] films is 800−825 °C. This illustrates that, in addition to composition and thickness, the film structure also influences film thermal stability. For a film with a homogeneous composition, increasing the thickness leads to decreased thermal stability as the surface energy makes less of a contribution to the total energy,[2,32,35] but for periodic structured films, the thicker film remains amorphous up to the same temperature that the thinner film can withstand, i.e., periodic films are thickness independent. On the other hand, the thicker homogeneous film without periodic structures will lose its thermal stability when annealed around the crystallization onset temperature of a thinner film. The absolute crystallization temperatures of the homogeneous films studied herein were higher than the periodic structured films since a large x value in [xHf + 1Al], resulting in a low incorporation level, was needed to ensure the existence of periodicity. Therefore, controlling the distribution of the incorporated Al can be an extra factor determining film thermal stability for Al-HfO_2 with a particular Al-incorporation level.

This structure dependent amorphization effect is not limited to the Al-HfO_2 system; ALD-grown La-HfO_2 (La-incorporated HfO_2) films change their phase in the same way, as shown in Figure 6. Similar AR-XPS analysis shows that the [6Hf + 1La] films are composed of periodic $HfLa_xO_y$ and HfO_2 layers, while [3Hf + 1La] films are more like homogeneous films.[36] The XPS peak positions and La-incorporation levels are reported elsewhere.[21] The 10 nm [3Hf + 1La] × 41 film remains amorphous after 900 and 925 °C, 30 s annealing, but the 40 nm [3Hf + 1La] × 160 film crystallizes after 700 °C, 30 s annealing (Figure 6a,b). The crystallization onset temperature of the [3Hf + 1La] films decreases from 925−950 to 650−700 °C as the film thickness increases from 10 to 40 nm. On the other hand, both the 10 nm [6Hf + 1La] × 22 and the 40 nm [6Hf + 1La] × 84 films can remain amorphous after a 825 °C, 30 s annealing (Figure 6c,d).

For homogeneous HfO_2-based ternary oxide thin films, there are two factors determining the film thermal stability: incorporated elements and overall film thickness. For instance, incorporating SiO_2, Al_2O_3, and La_2O_3 into HfO_2 is an effective method to increase the crystallization temperature,[9−22] and the crystallization temperature increases with higher incorporation levels, but for a fixed incorporated element concentration, thinner films have stronger thermal stability. In bulk materials, the crystalline phase is always thermodynamically more stable than the amorphous phase. However, amorphous phases usually have lower surface and interfacial energies in nanoparticles and thin films below some critical particle dimension or film thickness.[27,50,51] As homogeneous or homogeneous-like films (e.g., HfO_2, [3Hf + 1Al], [3Hf + 1La]) are made thinner, the surface energy contribution leads to a higher crystallization temperature, which makes the amorphous phase more stable. In other words, both

dx.doi.org/10.1021/cm102057d |*Chem. Mater.* 2011, 23, 1679–1685

film composition and overall film thickness affects the film thermal stability for homogeneous films.

On the other hand, thermal stability of an ALD-grown film with periodic structure tends to be independent of overall film thickness. A periodic structure can be considered as a stack composed of repeated ultrathin $HfM_xO_y-HfO_2$ layers (M stands for the incorporated element). In this study, the Al-HfO_2 films with high Hf:Al ALD cycle ratios are likely composed of repeated $HfAl_xO_y-HfO_2$ ultrathin layers since one ALD layer of Al_2O_3 only interacts with a limited number ALD layers of HfO_2, introducing numerous extra interfaces in the film. Although the surface enthalpy value of these interfaces may be different from that of the sample−air surface, the bulk energy may contribute less to the total energy in this case and the surface-to-volume ratio of an ultrathin layer is independent of film overall thickness. Thus, the crystallization temperature may be independent of total film thickness.

Ultrathin HfO_2 layers may become another factor determining film thermal stability for periodic films. Ultrathin HfO_2 can withstand a higher annealing temperature than thick HfO_2 films, maybe even thick HfO_2 incorporated with a weak amorphizer. Knowing that one ALD Al_2O_3 layer interacts with a limited number of ALD HfO_2 layers (about four layers by AR-XPS in this study), it is safe to conclude that varying Hf:Al ALD cycle ratio will only change the thickness of HfO_2 ultrathin layers in repeated $HfAl_xO_y-HfO_2$ structures, while the local Al concentration in the $HfAl_xO_y$ ultrathin layers remains relatively constant, as long as the Hf:Al ALD cycle ratio is in the range ensuring the existence of the $HfAl_xO_y-HfO_2$ periodic structure. Thus, the different crystallization temperatures of ALD-grown Al-HfO_2 films with different incorporation levels may essentially be determined by different thicknesses of ultrathin HfO_2 layers for periodic films, because HfO_2 layers are more likely to initiate the crystallization while $HfAl_xO_y$ layers tend to block the growth of the crystalline phase. As the thickness of $HfAl_xO_y$ and local Al concentration are fixed in all periodic $[x\mathrm{Hf} + 1\mathrm{Al}]$ films, we believe the different thicknesses of ultrathin HfO_2 layers in two periodic films, e.g., 10 nm $[8\mathrm{Hf} + 1\mathrm{Al}] \times 14$ and $[5\mathrm{Hf} + 1\mathrm{Al}] \times 21$, are the reason why the two films have different thermal stability. Therefore, tuning the thickness of the ultrathin host material in repeated layers might be an additional method to change the film crystallization temperature in various ALD-grown systems with a periodic structure.

4. CONCLUSION

The relationship between the thermal stability and the film structure of ALD-grown Al-HfO_2 films is studied. Ten nm Al-HfO_2 films with 8:1 and 3:1 AL:Hf ALD cycle ratios can remain amorphous after 800 and 900 °C annealing, respectively. Films with an Al:Hf ALD cycle ratio larger than four are found to be composed of periodic $HfAl_xO_y-HfO_2$ structures; the films are more like homogeneous mixtures when this ratio is equal to or less than three. For a $[3\mathrm{Hf} + 1\mathrm{Al}]$ structure, increasing film thickness lowers the thermal stability since the film is more homogeneous-like and the surface energy, which prefers the amorphous phase, plays less contribution to the total energy in the thicker film than it does in the thinner film. For a $[8\mathrm{Hf} + 1\mathrm{Al}]$ structure, the crystallization temperature is independent of film thickness because the surface-to-volume ratio remains constant as film thickness changes, which is caused by $HfAl_xO_y-HfO_2$ periodic structure. Therefore, the periodically repeated structure in an ALD-grown film is also an important factor determining the film thermal stability.

AUTHOR INFORMATION

Corresponding Author

*E-mail: ekerdt@che.utexas.edu. Telephone: 1-512-471-4689. Fax: 1-512-471-7060.

ACKNOWLEDGMENT

This work was supported by the National Science Foundation (Awards DMR-060646 and NNIN ECS-0335765).

REFERENCES

(1) Wilk, G. D.; Wallace, R. M.; Anthony, J. M. *J. Appl. Phys.* **2001**, *89*, 5243–5275.

(2) Gusev, E. P.; Cabral, C.; Copel, M.; D'Emic, C.; Gribelyuk, M. *Microelectron. Eng.* **2003**, *69*, 145–151.

(3) Kukli, K.; Aarik, J.; Uustare, T.; Lu, J.; Ritala, M.; Aidla, A.; Pung, L.; Harsta, A.; Leskela, M.; Kikas, A.; Sammelselg, V. *Thin Solid Films* **2005**, *479*, 1–11.

(4) Kukli, K.; Pilvi, T.; Ritala, M.; Sajavaara, T.; Lu, J.; Leskela, M. *Thin Solid Films* **2005**, *491*, 328–338.

(5) Hausmann, D. M.; Kim, E.; Becker, J.; Gordon, R. G. *Chem. Mater.* **2002**, *14*, 4350–4358.

(6) Mommer, N.; Lee, T.; Gardner, J. A. *J. Mater. Res.* **2000**, *15*, 377–381.

(7) Zhao, X.; Vanderbilt, D. *Phys. Rev. B.* **2002**, *65*, 233106/1–233106/4.

(8) Seo, M.; Min, Y.-S.; Kim, S. K.; Park, T. J.; Kim, J. H.; Na, K. D.; Hwang, C. S. *J. Mater. Chem.* **2008**, *18*, 4324–4331.

(9) Wilk, G. D.; Wallace, R. M.; Anthony, J. M. *J. Appl. Phys.* **2000**, *87*, 484–492.

(10) Tomida, K.; Kita, K.; Toriumi, A. *Appl. Phys. Lett.* **2006**, *89*, 142902/1–142902/3.

(11) Ohshita, Y.; Ogura, A.; Ishikawa, M.; Kada, T.; Hoshino, A.; Suzuki, T.; Machida, H.; Soai, K. *Chem. Vap. Deposition* **2006**, *12*, 130–135.

(12) Park, T. J.; Kim, J. H.; Jang, J. H.; Na, K. D.; Hwang, C. S.; Yoo, J. H. *Electrochem. Solid-State Lett.* **2008**, *11*, H121–H123.

(13) Lee, D.; Suh, D.; Pae, Y.; Kim, H.; Cho, M.-H.; Ko, D.-H. *J. Electrochem. Soc.* **2007**, *154*, H708–H712.

(14) Sivasubramani, P.; Kim, J.; Kim, M. J.; Gnade, B. E.; Wallace, R. M. *J. Appl. Phys.* **2007**, *101*, 114108/1–114108/4.

(15) Hoppe, E. E.; Aita, C. R. *Appl. Phys. Lett.* **2008**, *92*, 141912/1–141912/3.

(16) Marshall, P. A.; Potter, R. J.; Jones, A. C.; Chalker, P. R.; Taylor, S.; Critchlow, G. W.; Rushworth, S. A. *Chem. Vap. Deposition* **2004**, *10*, 275–279.

(17) Song, M.-K.; Kang, S.-W.; Rhee, S.-W. *J. Electrochem. Soc.* **2005**, *152*, C108–C112.

(18) Ho, M.-Y.; Gong, H.; Wilk, G. D.; Busch, B. W.; Green, M. L.; Lin, W. H.; See, A.; Lahiri, S. K.; Loomans, M. E.; Raisanen, P. I.; Gustafsson, T. *Appl. Phys. Lett.* **2002**, *81*, 4218–4220.

(19) Cho, M.-H.; Chang, H. S.; Cho, Y. J.; Moon, D. W.; Min, K.-H.; Sinclair, R.; Kang, S. K.; Ko, D.-H.; Lee, J. H.; Gu, J. H.; Lee, N. I. *Appl. Phys. Lett.* **2004**, *84*, 571–573.

(20) Yamamoto, Y.; Kita, K.; Kyuno, K.; Toriumi, A. *Appl. Phys. Lett.* **2006**, *89*, 032903/1–032903/3.

(21) Wang, T.; Ekerdt, J. G. *Chem. Mater.* **2009**, *21*, 3096–3101.

(22) Huang, L.-Y.; Li, A.-D.; Zhang, W.-Q.; Li, H.; Xia, Y.-D.; Wu, D. *Appl. Surf. Sci.* **2010**, *256*, 2496–2499.

(23) Toriumi, A.; Kita, K. In *Dielectric Films for Advanced Microelectronics*; Baklanov, M., Green, M., Maex, K., Eds.; John Wiley & Sons: Hoboken, NJ, 2007; p 297−336.

(24) Inoue, H.; Utsuno, F.; Yasui, I. *J. Non-Cryst. Solids.* **2004**, *349*, 16–21.

(25) Lucovsky, G.; Whitten, J. L. In *High Dielectric Constant Materials: VLSE MOSFET Applications*; Huff, H. R., Gilmer, D. C., Eds.; Springer: New York, 2005; p 311−358.
(26) Lee, C.-K.; Cho, E.; Lee, H.-S.; Hwang, C. S.; Han, S. *Phys. Rev. B* **2008**, *78*, 012102/1–012102/4.
(27) Ushakov, S. V.; Brown, C. E.; Navrotsky, A. *J. Mater. Res.* **2004**, *19*, 693–696.
(28) Yang, Z. K.; Lee, W. C.; Lee, Y. J.; Chang, P.; Huang, M. L.; Hong, M.; Yu, K. L.; Tang, M.-T.; Lin, B.-H.; Hsu, C.-H.; Kwo, J. *Appl. Phys. Lett.* **2007**, *91*, 202909/1–202909/3.
(29) Majumder, P.; Jursich, G.; Takoudis, C. *J. Appl. Phys.* **2009**, *105*, 104106/15–104106/6.
(30) Craciun, D.; Socol, G.; Axente, E.; Calca, A.-C.; Singh, R.; Craciun, V. *Mater. Res. Soc. Symp. Proc.* **2008**, *1074*, 1074–I03−18.
(31) Essary, C. R.; Ramani, K.; Craciun, V.; Singh, R. K. *Appl. Phys. Lett.* **2006**, *88*, 182902/1–182902/3.
(32) Cho, M. H.; Roh, Y. S.; Whang, C. N.; Jeong, K.; Nahm, S. W.; Ko, D.-H.; Lee, J. H.; Lee, N. I.; Fujihara, K. *Appl. Phys. Lett.* **2002**, *81*, 472–474.
(33) Cho, M.; Park, J.; Park, H. B.; Hwang, C. S.; Jeong, J.; Hyun, K. S. *Appl. Phys. Lett.* **2002**, *81*, 334–336.
(34) Park, T. J.; Kim, J. H.; Jang, J. H.; Lee, C.-K.; Na, K. D.; Lee, S. Y.; Jung, H.-S.; Kim, M.; Han, S.; Hwang, C. S. *Chem. Mater.* **2010**, *22*, 4175–4184.
(35) Navrotsky, A. *J. Mater. Chem.* **2005**, *15*, 1883–1890.
(36) Wang, T.; Ekerdt, J. G. *Chem. Mater.* **2010**, *22*, 3798–3806.
(37) Katamreddy, R.; Inman, R.; Jursich, G.; Soulet, A.; Takoudis, C. *Acta Mater.* **2008**, *56*, 710–718.
(38) Park, P. K.; Cha, E.-S.; Kang, S.-W. *Appl. Phys. Lett.* **2007**, *90*, 232906/1–232906/3.
(39) Moulder, J. F.; Stickle, W. F.; Sobol, P. E.; Bomben, K. D. *Handbook of X-ray Photoelectron Spectroscopy*; Physical Electronics, Inc.: Eden Prairie, MN, 1995.
(40) Zhu, W. J.; Tamagawa, T.; Gibson, M.; Furukawa, T.; Ma, T. P. *IEEE Electron Device Lett.* **2002**, *23*, 649–651.
(41) Streetman, B. G.; Banerjee, S. K. *Solid State Electronic Devices*, 6th ed.; Prentice Hall: Upper Saddle River, NJ, 2006; pp 154−168.
(42) Cho, M.-H.; Roh, Y. S.; Whang, C. N.; Jeong, K.; Choi, H. J.; Nam, S. W.; Ko, D.-H.; Lee, J. H.; Lee, N. I.; Fujihara, K. *Appl. Phys. Lett.* **2002**, *81*, 1071–1073.
(43) Toriumi, A.; Iwamoto, K.; Ota, H.; Kadoshima, M.; Mizubayashi, W.; Nabatame, T.; Ogawa, A.; Tominaga, K.; Horikawa, T.; Satake, H. *Microelectron. Eng.* **2005**, *80*, 190–197.
(44) Champaneria, R.; Mack, P.; White, R.; Wolstenholme, J. *Surf. Interface Anal.* **2003**, *35*, 1028–1033.
(45) Mack, P.; White, R.; Wolstenholme, J.; Conard, T. *Appl. Surf. Sci.* **2006**, *252*, 8270–8276.
(46) Chang, J. P.; Green, M. L.; Donnelly, V. M.; Opila, R. L.; Eng, J.; Sapjeta, J.; Silverman, P. J.; Weir, B.; Lu, H. C.; Gustafsson, T.; Garfunkel, E. *J. Appl. Phys.* **2000**, *87*, 4449–4455.
(47) Powell, C. J.; Jablonski, A. *NIST Electron Effective-Attenuation-Length Database*; Version 1; National Institute of Standards and Technology: Gaithersburg, MD, 2001.
(48) Kimura, K.; Nakajima, K.; Conard, T.; Vandervorst, W. *Appl. Phys. Lett.* **2007**, *91*, 104106/1–104106/3.
(49) Consiglio, S.; Mo, R. T.; Tai, T.-L.; Krishnan, S. A.; OMeara, D.; Wajda, C.; Chudzik, M. P. *ECS Trans.* **2007**, *6*, 167–177.
(50) Molodetsky, I. *J. Non-Cryst. Solids.* **2000**, *262*, 106–113.
(51) Pitcher, M. W.; Ushakov, S. V.; Navrotsky, A.; Woodfield, B. F.; Li, G.; Boerio-Goates, J.; Tissue, B. M. *J. Am. Ceram. Soc.* **2004**, *88*, 160–167.